2021

Effective Anisotropic Properties-Based Representation of Vapor Chambers

K. Baraya
Purdue University

J. A. Weibel
Purdue University, jaweibel@purdue.edu

S V. Garimella
University of Vermont, sureshg@purdue.edu

Effective Anisotropic Properties-Based Representation of Vapor Chambers

Kalind Baraya, Justin A. Weibel, and Suresh V. Garimella

Abstract— An easy-to-use representation of vapor chambers is developed in terms of effective anisotropic properties. This approach enables accurate simulation of the vapor chamber represented as a solid conduction block by assigning appropriate values to its effective density, specific heat, in-plane thermal conductivity, and through-plane thermal conductance. These effective properties are formulated such that the vapor chamber operation in terms of steady-state and transient thermal response matches a full, physical simulation of phase change and energy transport in the vapor core; they are intrinsic properties that can be applied independent of the boundary conditions and heat input.

Index Terms— **vapor chamber, heat pipe, thermal conductivity, transient, anisotropic**

I. INTRODUCTION

Vapor chambers are passive devices that utilize the latent heat of a working fluid to effectively spread heat from localized hotspots to larger surface areas [1–3]. Direct numerical and analytical simulation of the temperature response of vapor chambers [4–9] has involved prediction of the governing mass, momentum, and energy transport in the wick and vapor core, as well as coupling between these domains via evaporation and condensation. An alternative, and much more convenient, approach is to represent the wick and vapor core as solid blocks with appropriately assigned effective thermal properties, such that this proxy system can be simulated using conduction physics to obtain the correct transient and steady-state thermal response of a vapor chamber. Semi-empirical relations for the effective thermal properties of porous wicks are available in the literature [10]. For the vapor core, the effective thermal conduction properties must represent the actual physical processes of interfacial phase change and vapor flow. An effective *in-plane* (*x, y*) thermal conductivity for the vapor core is easily computed [11]; however, this property is not physically representative of *through-plane* (*z*) transport. No universal model parameter for through-plane effective thermal transport is available that yields an accurate prediction of vapor chamber temperatures.

In this work, we develop an effective anisotropic properties-based representation of the vapor core, which enables simulation of a vapor chamber as a conduction block to model its transient thermal response. The approach is verified against a validated time-stepping analytical model for vapor chamber transport [9] and exhibits excellent agreement across a wide range of operating and boundary conditions. The assumptions made in deriving these intrinsic effective properties are then used to formulate generalized expressions for estimating the error in thermal response *a priori*.

II. DERIVATION OF THE EFFECTIVE PROPERTIES

A. Thermal transport in the wall and wick

Heat transfer in the wall of a vapor chamber takes place via conduction and can be trivially represented by known solid properties. In the wick,

thermal transport occurs via conduction through the solid/liquid porous medium and advection due to liquid flow. Typical operating conditions result in a low Peclet number, and it is thus assumed that heat transport in the wick is primarily diffusive; advection is neglected [12]. Under these assumptions, the wick can be simulated via conduction in a solid block having the effective porous medium properties.

B. Thermal response of the vapor core

Two phenomena govern energy transport in the vapor core, namely, phase change at the wick–vapor interface and vapor flow.

Mass flux due to phase change at the wick–vapor interface is computed using kinetic theory,

$$m_{int}^{"} = \phi\left(T_{int} - T_{sat}\right)$$

$$\text{where } \phi = \frac{2\sigma}{2-\sigma}\frac{h_{fg}\rho}{T_{vap}^{1.5}}\left(\frac{1}{2\pi R}\right)^{0.5} \tag{1}$$

where all the symbols are defined in Table I.

Vapor transport is assumed to be incompressible, 2D, quasi-steady and diffusive, and described by

$$\frac{1}{\mu}\frac{\partial P}{\partial x} = \frac{\partial^2 u}{\partial z^2}; \ \frac{1}{\mu}\frac{\partial P}{\partial y} = \frac{\partial^2 v}{\partial z^2}. \tag{2}$$

The pressure in the vapor core is assumed to be uniform along the *z*-direction, therefore

$$u = \frac{1}{2\mu}\frac{\partial P}{\partial x}\left(z^2 - zh_{vap}\right); \ v = \frac{1}{2\mu}\frac{\partial P}{\partial y}\left(z^2 - zh_{vap}\right). \tag{3}$$

Integrating equation (3) along the *z* direction with no-slip boundary conditions at the wick–vapor core interfaces, and performing mass balance over an elementary control volume in the vapor core yields

$$\frac{\partial^2 P}{\partial x^2} + \frac{\partial^2 P}{\partial y^2} = \frac{-12\mu}{\rho h_{vap}^3}(m_{evap}^{"} + m_{cond}^{"}). \tag{4}$$

The saturation temperature in the vapor core is related to pressure using the Clausius-Clapeyron equation [13]. A linearized version of Clausius-Clapeyron equation is employed that assumes a constant gradient computed at a reference pressure and saturation temperature

$$\frac{dP}{dT_{sat}} = \frac{h_{fg}P_o}{R\left(\overline{T}_{sat}\right)^2}, \tag{5}$$

where the reference temperature is taken as the mean saturation temperature of the vapor core at any given point in time. Combining equations (4) and (5), and substituting the evaporation and condensation mass fluxes using equation (1), results in

$$\frac{h_{fg}^2 P \rho h_{vap}^2}{12R\mu\left(\overline{T}_{sat}^2\right)}\left(\frac{\partial^2 T_{sat}}{\partial x^2} + \frac{\partial^2 T_{sat}}{\partial y^2}\right) =$$

$$-\frac{\phi h_{fg} h_{vap}}{2}\left\{\frac{1}{h_{vap}}\left(\frac{T_{cond,int} - T_{sat}}{h_{vap}/2}\right) - \frac{1}{h_{vap}}\left(\frac{T_{sat} - T_{evap,int}}{h_{vap}/2}\right)\right\}. \tag{6}$$

The authors are with the Cooling Technologies Research Center, and the School of Mechanical Engineering, Purdue University, West Lafayette, IN 47907-2088 USA (kbaraya@purdue.edu; jaweibel@purdue.edu; sureshg@purdue.edu). The third author is currently President, University of Vermont.

C. Representation of vapor core transport as conduction in a solid

To simulate the thermal response of the vapor core as a conduction block, equation (6) is mapped to the proxy heat diffusion equation,

$$k_x\left(\frac{\partial^2 T_{\text{sat,p}}}{\partial x^2}\right)+k_y\left(\frac{\partial^2 T_{\text{sat,p}}}{\partial y^2}\right)=-k_z\left(\frac{\partial^2 T_{\text{sat,p}}}{\partial z^2}\right). \qquad (7)$$

where $T_{\text{sat,p}}$ is an analogous representation of the vapor core saturation temperature. Because equation (6) is derived by assuming that the pressure, and therefore the saturation temperature, in the vapor core along the z-direction is uniform, equation (7) is averaged along the z-direction resulting in

$$k_x\left(\frac{\partial^2 \overline{T}_{\text{sat,p}}}{\partial x^2}\right)+k_y\left(\frac{\partial^2 \overline{T}_{\text{sat,p}}}{\partial y^2}\right)=$$
$$-k_z\left\{\frac{1}{h_{vap}}\left(\frac{\partial T_{\text{sat,p}}}{\partial z}\right)_{z=h_{vap}}-\frac{1}{h_{vap}}\left(\frac{\partial T_{\text{sat,p}}}{\partial z}\right)_{z=0}\right\}. \qquad (8)$$

A comparison of the physical saturation temperature distribution, equation (6), with the left side of equation (8) shows that the effective thermal conductivity of the vapor core along x and y can be represented as

$$k_x=k_y=\frac{h_{fg}^2 P\rho h_{vap}^2}{12R\mu\overline{T}_{\text{sat}}^2}, \qquad (9)$$

which is consistent with the literature [11].

Furthermore, on comparing equation (8) to the right-hand side of equation (6), an effective conductance per unit length can be defined as a closed-form expression:

$$\text{conductance per unit length} = k_z=\frac{\phi h_{fg}h_{vap}}{2}. \qquad (10)$$

Note that k_z is not an effective thermal conductivity, but rather a conductance per unit length, and its magnitude is highly case-specific.

For simulating the transient behavior of the vapor core, the effective density ρ_{eff} and specific heat $C_{p,\text{eff}}$ of the solid conduction block representing the vapor core can be taken as the vapor properties.

$$\rho_{\text{eff}}=\rho;\ C_{p,\text{eff}}=C_p. \qquad (11)$$

The effective anisotropic properties k_x, k_y, k_z, along with ρ_{eff} and $C_{p,\text{eff}}$, can be specified in the simulation of conduction to yield the same steady and transient thermal response as a vapor core. These intrinsic properties depend only on the working fluid properties and vapor core thickness, and are independent of any boundary condition.

III. IMPLEMENTATION AND VERIFICATION

The effective anisotropic properties are verified by comparing the result of a conduction simulation using these effective anisotropic properties against an experimentally validated time-stepping analytical model for vapor chamber transport [9]. Two demonstration cases (Case 1 and Case 2) are considered that impose different boundary conditions on a vapor chamber of a fixed geometry. The temporal and spatial variation of temperatures on the evaporator and condenser surfaces are compared between the effective anisotropic properties-based representation and the physical vapor chamber model.

A. Implementation

Figure 1 shows the geometry of the vapor chamber used in Case 1 and Case 2, with wall, wick and vapor core thicknesses of 200 μm, 150 μm, and 200 μm, respectively. The wall and wick are each discretized into 800,000 computational cells, and the vapor core has 160,000 cells. The vapor core is meshed with a single element across its thickness, as shown in Figure 1. This is done to ensure that only a single computational node exists along the thickness of the vapor core at a

given planar location. This allows for solving an axially averaged saturation temperature in the vapor core. Using more than one computational node in the axial direction will lead to an axial gradient of saturation temperature in the vapor core. This will give an incorrect prediction because the expressions derived in equation (9), (10) and (11) are valid only for computing the axially averaged saturation temperature in the vapor core.

TABLE I: NOMENCLATURE

Symbol	Units	Symbol	Units
A	surface area (m^2)	R	gas constant (J kg^{-1} K^{-1})
C_p	specific heat (J kg^{-1} K^{-1})	Re	Reynolds number (-)
h_{fg}	enthalpy of vaporization (J kg^{-1})	r_{evap}	effective evaporator radius (m)
h_{vap}	vapor core thickness (m)	T	temperature (K)
k_x	thermal conductivity along x (W m^{-1} K^{-1})	T_o	operating temperature (K)
k_y	thermal conductivity along y (Wm^{-1}K^{-1})	$\overline{T}_{sat}$	vapor core mean T_{sat} (K)
k_z	thermal conductance per unit length along z (Wm^{-1}K^{-1})	u	velocity along x (m s^{-1})
L	length scale (m)	U_{max}	scale for velocity (ms^{-1})
m''	mass flux (kg m^{-2} s^{-1})	v	velocity along y (m s^{-1})
P	pressure in the vapor core (Pa)	x, y, z	coordinate axes
P_o	saturation pressure at T_o (Pa)	r	effective radius (m)
Q	power input (W)	ΔT_{sat}	T_{sat} drop in the vapor core
ΔP	pressure drop in the vapor core	$T_{sat,p}$	Representative T_{sat} (K)
q''	heat flux (Wm^{-2})	$\overline{T}_{sat,p}$	Axially averaged $T_{sat,p}$ (K)
$\Delta T_{sat,non-linear}$	ΔT_{sat} calculated using Clausius-Clapeyron equation (K)		

Subscripts			
cond	Condenser	int	interface
evap	Evaporator	vap	vapor
sat	Saturation	x, y, z	coordinate axis
eff	effective property	error	error induced in the quantity

Greek			
ϕ	Constant, Eq (1) (kg m^{-2} s^{-1} K^{-1})	ρ	vapor density (kg m^{-3})
σ	accommodation coefficient (-)	μ	vapor dynamic viscosity (Pa s)

The conduction simulations utilizing the effective anisotropic properties are implemented in ANSYS Fluent [14]. Copper is chosen as the material for modeling the walls as a solid conduction block. The solid conduction block used for modeling the wick is taken as a sintered copper with a porosity of 0.6 and thermal conductivity of 40 W/(mK), as in [9]. The vapor core is modeled as a solid block with effective properties as proposed in equations (9), (10), and (11). Water is used as the working fluid for both Case 1 and Case 2. Due to the temperature-dependence of the physical properties of the working fluid, the effective thermal properties of the vapor core are updated at each time-step based on the mean vapor core temperature. It should be noted that because the effective properties depend only on the physical design of the vapor chamber, the implementation of the effective properties is exactly the same for both Case 1 and Case 2. A second-order upwind scheme is used for spatial discretization, while a first-order implicit scheme is employed for temporal discretization of the heat diffusion equation. The time step for the solution is 0.2 s, with the vapor chamber initialized to $T = 300$ K at $t = 0$ s. The solution at each time step is considered converged when the residual falls below 1×10^{-12}.
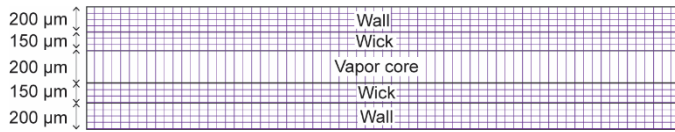
Figure 1. Illustration of the geometry and mesh of the vapor chamber considered. Note that the vapor core is meshed as a single layer for implementing the effective thermal conductance across the thickness.
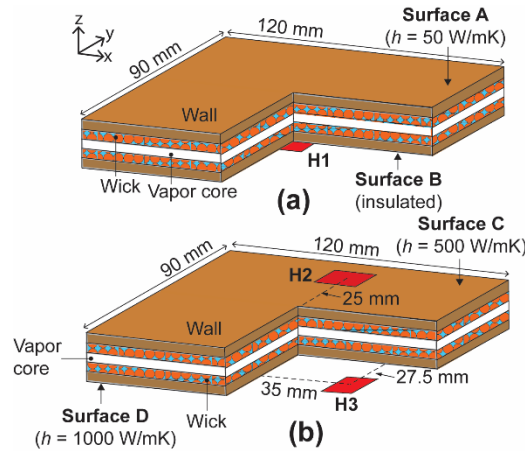

Figure 2. Vapor chamber boundary conditions used for verification of the effective anisotropic properties method: (a) Case 1 has a centrally located heat source with steady power generation on the otherwise insulated bottom-side Surface B and the top-side Surface A with a uniform heat transfer coefficient; (b) Case 2 has two eccentrically located and staggered heat sources with different heat transfer coefficients on Surface C and Surface D.
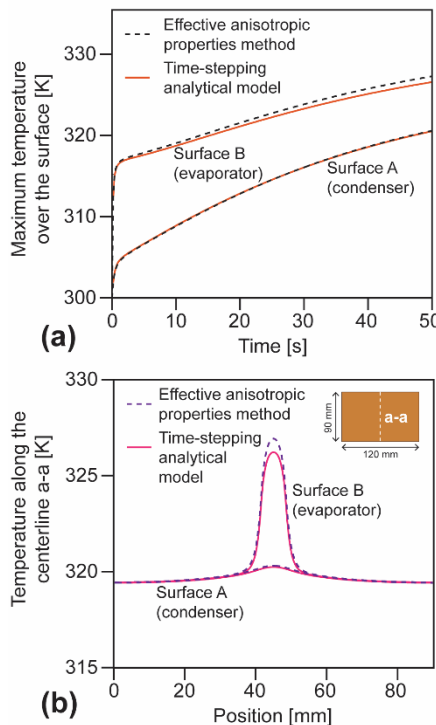

Figure 3. For Case 1: (a) transient maximum temperature rise and (b) spatial temperature profile on the Surface A (condenser) and Surface B (evaporator) at the end of 40 s.

For the purpose of verification, the same cases simulated via the effective-properties approach from the present study are also solved using the time-stepping analytical model as implemented in Ref. [9]. The validated model of a vapor chamber from Ref. [9] solves for thermal and hydraulic transport in the wall, vapor core, and wick. The model features a series solution in space for the governing equations and a forward marching scheme for obtaining the transient response.

B. Case 1: Centrally located heat source with steady power generation

A schematic diagram of the boundary conditions applied to the vapor chamber in Case 1 is shown in Figure 2 (a). The bottom side, Surface B, which acts as the evaporator in this case, is insulated except for a centrally located 7.2 mm × 7.2 mm heat source (H1; Q = 14 W). The top Surface A, which acts as the condenser surface, rejects heat to the ambient (300 K) with a heat transfer coefficient of 50 W/(m^{2}K).

Figure 3 compares the thermal response obtained using the effective anisotropic properties method (dashed lines) and the time-stepping analytical model (solid lines). Figure 3(a) plots the maximum temperature on the surfaces with time. Figure 3(b) shows the temperature profile along line a-a (shown in the inset) at the end of 40 s on both surfaces. The temporal and spatial temperature predictions are in excellent agreement, with a maximum deviation of only 0.7 K at the center of the evaporator at the end of 40 s using the effective through-plane conductance formulation for k_z per equation (10). For reference, this deviation is compared to two alternative representations of the through-plane transport (results not plotted in Figure 3). If k_z was instead assumed to be same as the effective in-plane thermal conductivity (k_x, k_y), i.e. isotropic, the deviation would increase to 7.0 K (underprediction). Or, if k_z was assumed equal to the gas thermal conductivity, this would result in a severe overprediction by 67.5 K.
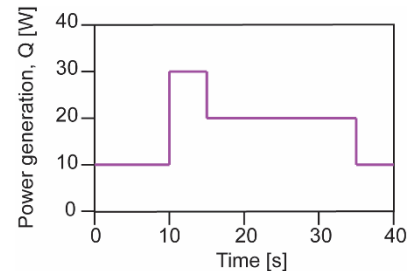

Figure 4. Time-varying power generation profile of heat source H2 in Case 2.

Case 2: Two eccentrically located and staggered heat sources with transient power generation

For Case 2, a mixed set of boundary conditions is used on both the bottom (Surface D) and top (Surface C) surfaces to demonstrate that the effective anisotropic properties are independent of any complex boundary conditions imposed. The positions of the heat sources on Surface C (H2, 10 mm × 5 mm, variable heat input) and Surface D (H3, 10 mm × 15 mm; Q = 15 W) are shown in Figure 2 (b). The power generation in heat source H2 varies with time as shown in Figure 4. All other exposed areas of Surface D and C reject heat to the ambient (300 K) with heat transfer coefficients of 1000 W/(m^{2}K) and 500 W/(m^{2}K), respectively.

Figure 5 shows a comparison of the transient thermal response for Case 2 using the effective properties method (dashed lines) and the time-stepping analytical model (solid lines). Figure 5(a) plots the variation of the transient maximum temperature for both surfaces, and Figure 5(b) shows the temperature profile along line a-a (shown in inset) at the end of 40 s. The temperature profile predicted using the

effective properties method shows an excellent match with the time-stepping analytical model. It is evident that the effective anisotropic properties method can predict the temporal and spatial temperature variation with good accuracy compared to the time-stepping analytical model, even in the cases where non-uniform time-varying boundary conditions exist. The maximum deviation in the prediction of spatial temperature distribution is only 0.16 K for this case. It should be noted that the relative difference in temperatures between the two models is highly case-specific, but this nevertheless demonstrates excellent agreement for a relatively complex scenario.
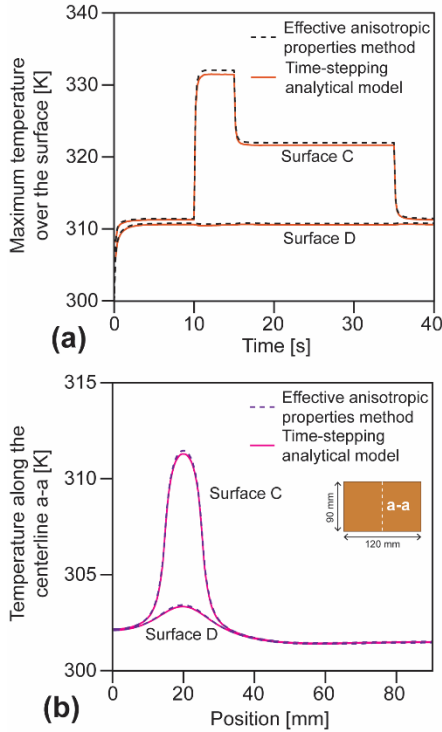

Figure 5. For Case 2: (a) transient maximum temperature rise and (b) spatial temperature profile on Surfaces C and D at the end of 40 s.

IV. SCALING-ANALYSIS-BASED ERROR ESTIMATION

Several key assumptions were required to derive the effective properties, the validity of which depends on the given heat load and vapor core thickness. Expressions for the estimated errors in predicted thermal response due to each assumption are derived based on scaling analyses in this section. These expressions can be evaluated to estimate error for any vapor chamber case independently, without requiring comparison to a full vapor chamber model. For each assumption, the error term is defined as the ratio of the magnitude of error in saturation temperature drop to the total temperature difference across the vapor core,

$$\text{error} = \frac{\Delta T_{\text{sat,error}}}{\Delta T_{\text{sat}} + q''/\phi h_{\text{fg}}} . \tag{12}$$

The total temperature difference across the vapor core (denominator) is approximated as the sum of the saturation temperature drop in the vapor core and the maximum wick–vapor core interfacial temperature difference from equation (1). The definition of error in equation (12) will give an upper bound on the relative error in temperature prediction, as the total temperature drop across the vapor chamber will actually be higher than the temperature drop across the vapor core, resulting in a lower relative error.

A. Assumption 1: Neglecting convective transport in the vapor core

In the derivation of the effective properties for vapor core transport, it is assumed that the contribution from convective transport is negligible compared to the diffusive transport. An error estimate is required for the case where convective transport in the vapor core is comparable. The error is estimated by first estimating the error in the pressure drop in the vapor core, and then relating this error in pressure drop to the error in temperature drop using the linearized Clausius-Clapeyron equation.

To estimate the error in pressure drop for the case with comparable convective transport in the vapor core, it can be assumed that the non-dimensional convective and diffusive transport terms are of the same order. Therefore, the scale of error in the pressure drop by neglecting convective terms can be expressed as

$$\Delta P_{\text{error}} \sim \left(2 \text{Re}_{i,\text{vap}} \frac{h_{\text{vap}}^2}{L_i} \right) \Delta P \; ; i = x, \, y$$

$$\text{where } \text{Re}_i \equiv \frac{\rho U_{\text{max}} L_i}{\mu} \text{ and } L_i = 2\sqrt{A_{evap}/\pi} \; . \tag{13}$$

The error term given by equation (13) is proportional to the pressure drop in the vapor core. Thus, to get an approximation of pressure drop in the vapor core, equation (3) is evaluated at $z = h_{\text{vap}}/2$

$$\Delta P \approx \frac{8\mu U_{\text{max}} L_i}{h_{\text{vap}}^2}; \, i = x, \, y \; . \tag{14}$$

Here, U_{max} is an estimation of the centerline velocity of the vapor flow, and can be approximated from mass conservation over the vapor core cross-sectional area in the evaporator region as

$$U_{\text{max}} \approx \frac{Q}{\left(2\pi r_{\text{evap}} \right)\left(h_{\text{vap}} \rho h_{\text{fg}} \right)} \; . \tag{15}$$

where r_{evap} is the effective evaporator radius given as $\sqrt{A_{evap}/\pi}$. Substituting equation (15) into (14), the pressure drop in the vapor core can be approximated as

$$\Delta P \approx \frac{4\mu Q L_i}{\pi \rho h_{\text{fg}} r_{\text{evap}} h_{\text{vap}}^3} \; . \tag{16}$$

Using the linearized Clausius-Clapeyron equation, the corresponding saturation temperature drop is approximated from equation (16), as

$$\Delta T_{\text{sat}} \approx \left(\frac{4\mu q''}{\pi h_{\text{vap}}^2 \rho h_{\text{fg}}} \sqrt{A_{\text{evap}} A_{\text{cond}}} \right) \frac{R T_o^2}{h_{\text{fg}} P_o} \; . \tag{17}$$

Hence, using equations (13), (16) and (17), and the definition of error as given in equation (12), error in the vapor core saturation temperature drop due to neglecting convective transport, as a fraction of total temperature difference across the vapor core is

$$\text{error} = \left(2 \text{Re}_i \frac{h_{\text{vap}}^2}{L_i^2} \right) \left(\frac{\Delta T_{\text{sat}}}{\Delta T_{\text{sat}} + q''/\phi h_{\text{fg}}} \right)$$

$$\text{where } \text{Re}_i \frac{h_{\text{vap}}^2}{L_i^2} \approx \frac{q'' h_{\text{vap}}}{4\mu h_{\text{fg}}} \sqrt{\frac{A_{\text{evap}}}{A_{\text{cond}}}} \; . \tag{18}$$

B. Assumption 2: Linearizing the Clausius-Clapeyron equation

In the derivation of the effective properties, a linearized version of the Clausius-Clapeyron equation is used to relate pressure to the saturation temperature drop in the vapor core. The linearized Clausius-Clapeyron equation is valid for cases when the temperature range over which the linear approximation is applied is comparable to the reference temperature. Hence, if the predicted temperature drop in the vapor core fails to meet the validity criterion of the linearized Clausius-Clapeyron equation, an estimation of the error induced in the predicted thermal

response of the vapor chamber is required. The absolute magnitude of error in predicted temperature will be

$$\Delta T_{\text{sat,error}} = \Delta T_{\text{sat}} - \Delta T_{\text{sat,non-linear}} \cdot \qquad (19)$$

where ΔT_{sat} is the predicted temperature drop in the vapor core using the linearized Clausius-Clapeyron equation from equation (17) and $\Delta T_{\text{sat,non-linear}}$ is the temperature drop in the vapor core without linearizing the Clausius-Clapeyron equation. If P_o is the saturation pressure at the operating temperature of the vapor chamber T_o, then the temperature drop in the vapor core without linearizing the Clausius-Clapeyron equation can be approximated as

$$\Delta T_{\text{sat,non-linear}} \approx T_{\text{sat}}\big|_{P_{\text{sat}} = P_O + \Delta P} - T_o, \qquad (20)$$

where ΔP is the pressure drop in the vapor core approximated from equation (16). Using the definition of error from equation (12), the error in the vapor core saturation temperature drop, due to the linearization, is defined as

$$\text{error} = \frac{\Delta T_{\text{sat}} - \Delta T_{\text{sat, non-linear}}}{\Delta T_{\text{sat}} + q''/\phi h_{\text{fg}}} \cdot \qquad (21)$$

C. Error evaluation

The error expressions (equations (18), (21)) are functions of the maximum heat flux, heat source and vapor chamber footprint area, vapor core thickness, fluid properties, and operating temperature. It is important to note that all these parameters are available without any need for resorting to simulations, and the error can be assessed from known conditions and parameters. This allows a user to judge whether the effective properties method provides an accurate prediction *a priori*.

The errors are explored now with varying vapor core thickness and input heat flux at T_o = 325 K. The heat source and vapor chamber footprint areas are taken for the example of Case 1 with water as the working fluid.

Figure 6(a) plots contours of the percentage error in the saturation temperature drop induced by neglecting convective transport in the vapor core. The error in the specific heat flux and vapor core thickness from Case 1 is only 2.2 % of the total temperature difference of the vapor core. More generally, the plot also shows that the error induced is relatively smaller at lower heat fluxes; lower vapor velocities (due to lower heat flux) facilitate diffusive transport in the planar direction. There is a non-monotonic trend in the error with the vapor core thickness. At smaller thicknesses, the diffusive transport in the vapor core becomes a better assumption. At very large vapor core thicknesses, convective transport is not negligible compared to diffusive transport, but the magnitude of error induced becomes a smaller fraction of total temperature difference of the vapor core. These opposing trends lead to the error being a maximum at some intermediate thickness.

The error induced in prediction of the saturation temperature drop due to linearizing the Clausius-Clapeyronon equation is plotted as a function of vapor core thickness and heat flux in Figure 6(b). For the specific parameters of Case 1, the error induced is 0.7 %. The error can become large at very small thickness for which there is large temperature drop in the vapor core, such that the linearized Clausius-Clapeyron equation is no longer a valid assumption.

It is recommended that these error terms be evaluated for each case of interest where the effective-properties simulation is to be applied. Even with this caution, the errors shown in Figure 6 indicate that the effective properties-based representation accurately captures the physics of vapor chamber thermal transport, providing a more

appropriate prediction than representing a vapor core by isotropic conduction.
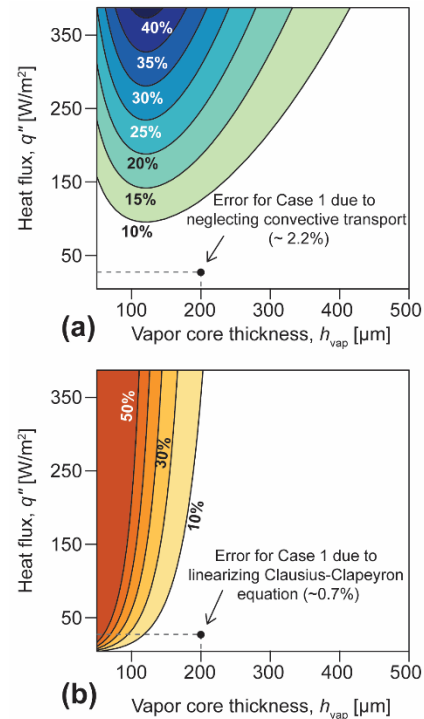

(a)

(b)

Figure 6. Percent errors, shown as contour maps as a function of the input heat flux and vapor core thickness, due to (a) neglecting convective transport in the vapor core and (b) linearizing the Clausius-Clapeyron equation. The error in the thermal response computed for Case 1 is indicated using a solid dot.

V. CONCLUSION

This paper demonstrates accurate simulation of vapor chamber thermal transport as conduction in a solid block represented by effective thermal anisotropic properties. The intrinsic effective properties derived depend only on the working fluid properties and vapor core thickness, and are independent of boundary condition. Expressions are formulated to allow estimation of the error associated with use of these effective properties before running a simulation, enabling a user to determine the suitability of this approach for a particular vapor chamber and the conditions of interest.

REFERENCES

[1]   R. Mahajan, C.P. Chiu, and G. Chrysler, "Cooling a Microprocessor Chip," *Proceedings of the IEEE*, vol. 94, 2006, pp. 1476–1486.

[2]   A. Bar-Cohen and P. Wang, "Thermal Management of On-Chip Hot Spot," *ASME Journal Of Heat Transfer*, vol. 134, 2012, pp. 553–567.

[3]   J.A. Weibel and S. V. Garimella, "Recent Advances in Vapor Chamber Transport Characterization for High-Heat-Flux Applications," *Advances in Heat Transfer*, vol. 45, 2013, pp. 209–301.

[4]   J.M. Tournier and M.S. El-Genk, "A Heat Pipe Transient Analysis Model," *International Journal of Heat and Mass Transfer*, vol. 37, 1994, pp. 753–762.

[5]   Y. Wang and K. Vafai, "Transient Characterization of Flat Plate Heat Pipes during Startup and Shutdown Operations," *International Journal of Heat and Mass Transfer*, vol. 43, 2000, pp. 2641–2655.

[6]   U. Vadakkan, S. V. Garimella, and J. Murthy, "Transport in

Flat Heat Pipes at High Heat Fluxes From Multiple Discrete Sources," *ASME Journal Of Heat Transfer*, vol. 126, pp. 347–354.

[7] R. Rullière, F. Lefèvre, and M. Lallemand, "Prediction of the Maximum Heat Transfer Capability of Two-phase Heat Spreaders - Experimental Validation," *International Journal of Heat and Mass Transfer*, vol. 50, 2007, pp. 1255–1262.

[8] Y. Yadavalli, J.A. Weibel, and S. V. Garimella, "Performance-Governing Transport Mechanisms for Heat Pipes at Ultra-thin Form Factors," *IEEE Transactions on Components, Packaging and Manufacturing Technology*, vol. 5, 2015, pp. 1618–1627.

[9] G. Patankar, J.A. Weibel, and S. V. Garimella, "A Validated Time-stepping Analytical Model for 3D Transient Vapor Chamber Transport," *International Journal of Heat and Mass Transfer*, vol. 119, 2018, pp. 867–879.

[10] D.A. Reay, P.A. Kew, and R.J. McGlen, *Heat Pipes*, Elsevier, 2014.

[11] R.S. Prasher, "A Simplified Conduction Based Modeling Scheme for Design Sensitivity Study of Thermal Solution Utilizing Heat Pipe and Vapor Chamber Technology," *Journal of Electronic Packaging*, vol. 125, 2003, p. 378.

[12] M. Kaviany, *Principles of Heat Transfer in Porous Media*, New York, NY (United States): Springer Science & Business Media, 2012.

[13] Y.A. Cengel and M.A. Boles, *Thermodynamics : an Engineering Approach*, Boston: McGraw-Hill Higher Education, 2006.

[14] Fluent, "ANSYS FLUENT 14. 0 User's Guide," *Ansys INC*, Canonsburg, PA: 2009.

Kalind Baraya received the B.Tech in Mechanical Engineering from IIT, Guwahati in 2012. He is a currently a PhD student under the advisement of Dr. Justin A. Weibel and Dr. Suresh V. Garimella in the Cooling Technologies Research Center, School of Mechanical Engineering, Purdue University, West Lafayette, IN. His research focuses on modeling and experimental characterization of vapor chambers and heat pipes, with emphasis on designing vapor chambers operating under steady state, transient, and dryout-recovery conditions.

Justin A. Weibel is a Research Associate Professor in the School of Mechanical Engineering at Purdue University and Director of the Cooling Technologies Research Center (CTRC), a graduated NSF I/UCRC. He received his PhD in 2012 and BSME in 2007, both from Purdue University. Dr. Weibel's research explores methodologies for prediction and control of heat transport to enhance the performance and efficiency of thermal management technologies and energy transfer processes. Dr. Weibel has supervised over 30 PhD and MS students and co-authored over 130 referred journal and conference papers. He was recently recognized as an Outstanding Engineering Teacher by the College of Engineering at Purdue University and received the 2020 ASME Electronic & Photonic Packaging Division (EPPD) Young Engineer Award. He is an Associate Editor of the IEEE Transactions on Components Packaging and Manufacturing Technology.

Suresh V. Garimella is currently President of the University of Vermont (UVM), Professor in Department of Mechanical Engineering at UVM, and Distinguished Professor Emeritus of Mechanical Engineering at Purdue University, where he founded the National Science Foundation Cooling Technologies Research Center. He has supervised over 90 Ph.D. and M.S. students, has co-authored 525 refereed journal and conference publications, and holds 13 patents. Twenty-eight alumni from his research group are now faculty members at prestigious universities around the world. His research group has made seminal contributions to micro and nanoscale thermal and fluidic engineering, novel materials for thermal management, materials processing and manufacturing, and renewable energy. Dr. Garimella is a Member of the National Science Board (NSB) and Fellow of the National Academy of Inventors, and of AAAS and ASME. His contributions to thermal management have been recognized with the 2016 ITherm Achievement Award, 2010 Heat Transfer Memorial Award, and 2009 Allan Kraus Thermal Management Medal.